PHYSICAL REVIEW B **90**, 241103(R) (2014)

Controlling multipolar radiation with symmetries for electromagnetic bound states in the continuum

Thomas Lepetit and Boubacar Kanté*

Department of Electrical and Computer Engineering, University of California San Diego, La Jolla, California 92093-0407, USA

(Received 5 June 2014; revised manuscript received 13 November 2014; published 1 December 2014)

Interferences in open systems embedded in a continuum can lead to states that are bound within the continuum itself. An electromagnetic state that naturally decays becomes bound at a unique point in phase space. We demonstrate the striking occurrence of multiple such peculiar states in coupled deep subwavelength resonators. The bound states in the continuum originate from the control of multipolar radiation and their symmetries. The architectures investigated here, using all-dielectric resonators, constitute a flexible and readily achievable platform for applications requiring strong light-matter interaction and light localization.

DOI: 10.1103/PhysRevB.90.241103 PACS number(s): 81.05.Zx, 41.20.Jb, 42.25.Bs, 78.20.Ci

Controlling the quality factor of cavities is of fundamental importance in electromagnetism, from microwaves to optics, for devices spanning oscillators, filters, antennas, sensors, nanolasers, or single-photon sources [1–4]. Quality factors are usually limited by ohmic, dielectric, and radiation losses. While the first two types of losses depend mostly on inherent material properties, the last one can be efficiently controlled. Several solutions have been investigated towards that end, including whispering gallery modes [5], photonic crystal cavities [6], negative index heterostructures [7], and, more recently, bound states in the continuum (BICs). In 1929, von Neumann and Wigner showed theoretically that certain quantum systems can surprisingly have bound states above the continuum threshold [8]. States above threshold, thus coupled to the outside, can be described by non-Hermitian Hamiltonians on account of their nonconservative nature [9]. In open systems, bound states are usually turned into resonances with a complex energy, $E = E_R + jE_I$. BICs are peculiar states with a vanishing imaginary part [10].

In photonics, these states have been shown to exist in dielectric gratings [11], photonic crystal cavities [12], lossless core-shell particles [13], coupled waveguide arrays [14–18], and photonic crystal slabs [19]. However, all reported electromagnetic systems have only exhibited single BICs. A single such state, usually a needle in a haystack, is extremely sensitive to perturbations. A small change in parameters usually leads to the disappearance of the mode in phase space. A fundamental question is thus to know whether there exist geometries in which the phase space can exhibit quasidegenerate BICs. Having several BICs in a small neighborhood of parameter space would make the system robust. In this Rapid Communication, we demonstrate the striking existence of multiple BICs in deeply subwavelength all-dielectric resonators. We show specifically that coupling in and among electromagnetic multipoles leads to the formation of several BICs closely spaced in phase space.

Our system represents a robust, ideal, and flexible platform to investigate the physics of open systems with controllable complex energies. These results bring BICs a significant step closer to the myriad of applications requiring strong light-matter interaction and light localization such as biosensing and photovoltaics.

*bkante@ucsd.edu

Periodic structures such as photonic crystals and metamaterials can be investigated at the unit cell level. An infinite array is equivalent to a waveguide with periodic boundary conditions loaded by a scatterer. The scattering problem thus reduces to a waveguide two-port problem [Fig. 1(a)]. In this picture, incoming and outgoing waves (waveguide modes) serve to probe resonances occurring in the internal domain via ports. Borrowing from nuclear physics [20–23], such an experiment can be described by a non-Hermitian effective Hamiltonian $\mathbf{H}_{\text{eff}}$ that is related to the scattering matrix $\mathbf{S}$ by

$$\mathbf{S} = \mathbf{C} - j\mathbf{V}[\omega\mathbf{I} - \mathbf{H}_{\text{eff}}]^{-1}\mathbf{V}^{\dagger}, \tag{1}$$

$$\mathbf{H}_{\text{eff}} = \mathbf{H}_{\text{QQ}} + j\tfrac{1}{2}\mathbf{V}\mathbf{V}^{\dagger}. \tag{2}$$

$\mathbf{H}_{\text{QQ}}$ is the Hamiltonian of the internal domain, $\mathbf{V}$ is the coupling matrix, and $\mathbf{C}$ is the direct pathway scattering matrix [24]. The fact that the latter can be different from unity results in characteristically asymmetric Fano line shapes [25]. From Eq. (1), the eigenvalues of the effective Hamiltonian can be retrieved from the poles of the scattering matrix. Alternatively, Siegert boundary conditions can be used instead of the effective Hamiltonian approach [26,27]. Generally, the effective Hamiltonian depends on a number of parameters and eigenvalues thus exist in a hyperspace. However, in a given frequency range, the investigation can be reduced to a finite number of resonances and parameters, limiting the complexity of the effective Hamiltonian. In non-Hermitian systems, when two eigenvalues come close to crossing as a function of a parameter, an avoided resonance crossing (ARC) occurs, i.e., eigenvalues repel each other in the entire complex plane [28–31]. As first shown by Friedrich and Wintgen [10], BICs based on destructive interferences represent a particular type of ARC for which coupling occurs predominantly in the far field [21].

We consider a rectangular metallic waveguide loaded with a single scatterer, which is a configuration closely related to microwave quantum billiards [32]. The system is equivalent to measuring a periodic array illuminated by a plane wave incident at an angle. In the X band (7–13 GHz), only one continuum is open (TE_{01} mode), the next higher-order continuum (TE_{02} mode) being cutoff below 13.12 GHz. The scatterer is a cylinder made of a high-permittivity, low-loss ceramic ($\varepsilon_r = 43$, $Q \times f = 41\,000$). Two variations on this resonator are used to investigate ARCs. We first consider

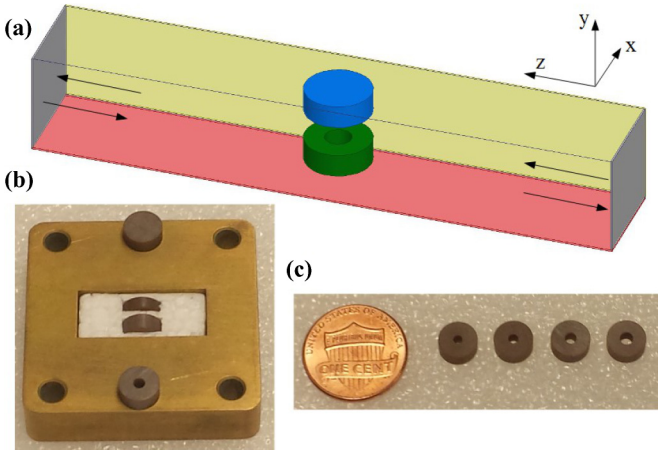

FIG. 1. (Color online) (a) Two-port waveguide configuration equivalent to a metamaterial array. Ports are depicted in gray. (b) Fabricated high-permittivity ceramic cylinders without a hole (resonator 1, top) and with a hole (resonator 2, bottom) and their sample holder. (c) Set of four cylinders with a different inner diameter (0.05″–0.08″).

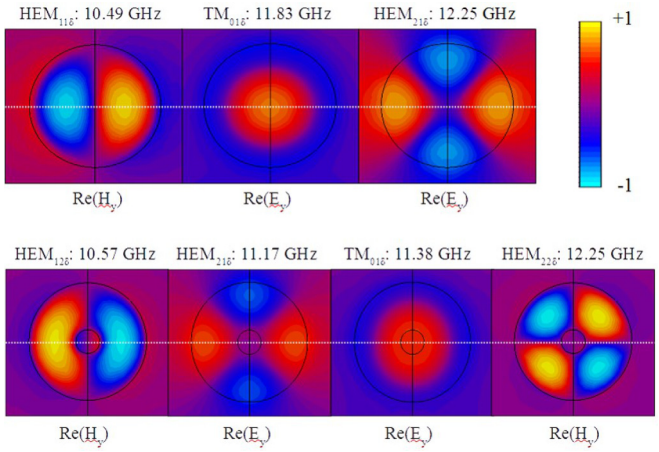

FIG. 2. (Color online) Normalized electric and magnetic fields in the *Oxz* plane [see Fig. 1(a)]. Top: Top view of resonator 1 (without hole). Bottom: Top view of resonator 2 (with hole) for all seven resonant modes.

resonator 1 on its own, with a radius of 3.5 mm and a height of 2.5 mm [Fig. 1(b)]. We find that three distinct resonances exist between 10.3 and 12.6 GHz, and their frequencies, quality factors, and symmetries are reported in Table I. Using the Kajfez and Guillon's nomenclature [33], the lowest to highest frequency modes are identified to be the transverse magnetic dipole ($HEM_{11\delta}$), the axial electric dipole ($TM_{01\delta}$), and the transverse magnetic quadrupole ($HEM_{21\delta}$). The symbol δ denotes the fact that the index along z is not an integer in dielectric resonators.

We now consider resonator 2 on its own, with a radius of 3.5 mm, a height of 3.0 mm, and an inner radius of 0.71 mm [Fig. (1b)]. Four distinct resonances are found, and their frequencies, quality factors, and symmetries are reported in Table I. Two new modes appear compared to the case of resonator 1: the transverse electric dipole ($HEM_{12\delta}$) and the transverse electric quadrupole ($HEM_{22\delta}$). Coupling between modes in the far field can happen only if they have the same symmetry with respect to the *Oxy* plane [Fig. 1(a)]. Consequently, from Table I, the two highest order modes of resonator 1 and the three highest order modes of resonator 2 can couple. The field distribution of the different modes is presented in Fig. 2.

TABLE I. Resonance frequencies, Q factors, and symmetries of modes (with respect to the *Oxy* plane). The first three modes belong to resonator 1 (without hole), while the last four modes belong to resonator 2 (with hole).

Mode	F (GHz)	Q ($F/\Delta F$)	*Oxy* symmetry
$HEM_{11\delta}$	10.49	7	Odd
$TM_{01\delta}$	11.83	21	Even
$HEM_{21\delta}$	12.25	217	Even
$HEM_{12\delta}$	10.57	105	Odd
$HEM_{21\delta}$	11.17	134	Even
$TM_{01\delta}$	11.38	17	Even
$HEM_{22\delta}$	12.25	1667	Even

ARCs in resonator 1 alone are investigated by varying its height. We compute the scattering matrix, using full-wave finite-element simulations, and extract its complex poles [21]. Resonance frequencies, plotted in Fig. 3 as a function of cylinder height, show a quasilinear dependence for all modes. The height is thus an inadequate parameter to obtain ARCs. Considering the in-plane electric field distribution of Fig. 2, perturbation theory indicates that drilling a hole in the center of the cylinder should only shift certain resonances. Resonance frequencies, plotted in Fig. 3 as a function of the inner radius, show that the $TM_{01\delta}$ mode is shifted to higher frequencies while the $HEM_{21\delta}$ mode is barely affected. A crossing of these two modes is observed for a radius of about 0.53 mm.

In the following, we use the flat continuum hypothesis, i.e., we neglect the frequency dependence of waveguide modes around resonances [21]. The $HEM_{22\delta}$ mode being spectrally separated from other modes of even parity in resonator 2, we can describe the system between 11.0 and 11.6 GHz by the

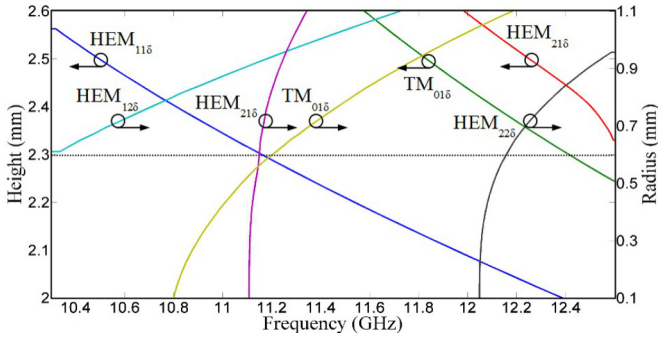

FIG. 3. (Color online) Real part of the S-matrix poles, resonance frequencies, as a function of the height (resonator 1) and as a function of the radius (resonator 2). Circles are frequencies at which fields are plotted in Fig. 2. The dashed line denotes the height of resonator 1 chosen in the coupled resonators configuration.

effective Hamiltonian

$$\mathbf{H}_{\text{eff}} = \begin{pmatrix} \omega_1 & 0 \\ 0 & \omega_2 \end{pmatrix} + j\frac{1}{2}\begin{pmatrix} 2\gamma_1 & 2\sqrt{\gamma_1\gamma_2} \\ 2\sqrt{\gamma_1\gamma_2} & 2\gamma_2 \end{pmatrix}, \quad (3)$$

where ω_n and γ_n are the resonance frequencies and linewidths of the uncoupled modes, respectively. In this system, irrespective of the coupling strength $\sqrt{\gamma_1\gamma_2}$, real parts of eigenvalues always cross while imaginary parts repel each other. At the crossing point, eigenvalues verify $\text{Im}(\omega_+) = \gamma_1 + \gamma_2$ and $\text{Im}(\omega_-) = 0$. One of the resonances becomes short lived while the other one becomes long lived to the point where it is no longer coupled to the continuum. In nuclear physics, this phenomenon is known as resonance trapping [9] while in electromagnetism it is known as bound states in the continuum [11].

In our system, we observe a striking appearance of a mode with a quality factor of 1646 at a radius of 0.53 mm (not shown). The incomplete decoupling from the continuum, as testified by the finite quality factor, stems from the ceramic finite loss tangent ($\tan\delta = 2e^{-4}$) and from a residual off-diagonal contribution from the principal value integral [21,30].

We now propose a system exhibiting multiple BICs. Resonators 1 and 2, separated by a distance of 1.5 mm as illustrated in Fig. 1, are considered. Near-field coupling can now occur in addition to far-field coupling. Rigorously, the open system should be described by a 7×7 effective Hamiltonian. However, for two resonances that are spectrally separated from others and close to an ARC the effective Hamiltonian can be written

$$\mathbf{H}_{\text{eff}} = \begin{pmatrix} \omega_1 & \kappa \\ \kappa^* & \omega_2 \end{pmatrix} + j\frac{1}{2}\begin{pmatrix} 2\gamma_1 & 2\sqrt{\gamma_1\gamma_2} \\ 2\sqrt{\gamma_1\gamma_2} & 2\gamma_2 \end{pmatrix}, \quad (4)$$

where κ is the near-field coupling constant. $\mathbf{H}_{\text{QQ}}$ is Hermitian because the closed system (resonators 1 and 2) is conservative. In the open system, real and imaginary parts of eigenvalues cross or repel depending on the relative coupling strengths $\sqrt{\gamma_1\gamma_2}$ and κ. BICs are thus still possible but do not necessarily occur exactly at the crossing point due to near-field coupling [21].

To obtain multiple BICs, the height of resonator 1 is set to 2.3 mm (Fig. 3, dashed line) and the inner radius of resonator 2 is varied from 0.1 to 1.1 mm. Figure 4 shows the reflection spectrum between 10.35 and 12.6 GHz, where three resonances with vanishing widths or BICs are clearly seen. BICs occur when reflection and transmission zeroes exactly coincide [34].

To understand their origin, resonance frequencies are plotted as a function of the inner radius in Fig. 5. Six modes occur between 10.35 and 12.6 GHz, the $\text{HEM}_{21\delta}$ mode being outside that frequency range. Five ARCs take place.

At 12.39 GHz and 0.95 mm, modes $\text{TM}_{01\delta}(1)$ and $\text{HEM}_{22\delta}(2)$ cross, the number in parentheses indicating the resonator to which the mode belongs. They can couple both in the near field, because they belong to different resonators, and in the far field, because they have the same symmetry. At 11.11 GHz and 0.51 mm, modes $\text{TM}_{01\delta}(2)$ and $\text{HEM}_{21\delta}(2)$ cross. They can only couple in the far field. At 11.17 GHz and 0.82 mm, modes $\text{HEM}_{12\delta}(2)$ and $\text{HEM}_{21\delta}(2)$ cross. They cannot couple at all. The last two ARCs are more complex because they involve the $\text{HEM}_{11\delta}(1)$ mode which has a very low-quality factor ($Q = 7$). In the presence of resonator 2 this mode is shifted from 11.14 GHz (uncoupled resonator in Fig. 3) to about 10.87 GHz (coupled resonator in Fig. 5). Therefore, unlike what would be predicted from Fig. 3, it does not couple to mode $\text{HEM}_{21\delta}(2)$. However, it still couples to mode $\text{TM}_{01\delta}(2)$ at 10.88 GHz and 0.24 mm (near-field coupling) and mode $\text{HEM}_{12\delta}(2)$ at 10.70 GHz and 0.72 mm (near- and far-field couplings). Around that last ARC, resonance frequencies repel because the near-field coupling is very strong due to the low confinement of the $\text{HEM}_{11\delta}(1)$ mode ($Q = 7$). Such a phenomenon is not witnessed for other ARCs involving near-field coupling because they occur outside of the parameter range for radius larger than 1.1 mm. Among those five ARCs three involve far-field coupling and BICs are thus expected. The $\text{HEM}_{12\delta}$, $\text{HEM}_{21\delta}$, and $\text{HEM}_{22\delta}$ modes become long lived reaching quality factors of the order of 1700 as can be seen in Fig. 6. This system thus exhibits multiple BICs in a neighborhood of parameter space (inner radius) making it less sensitive to perturbations.

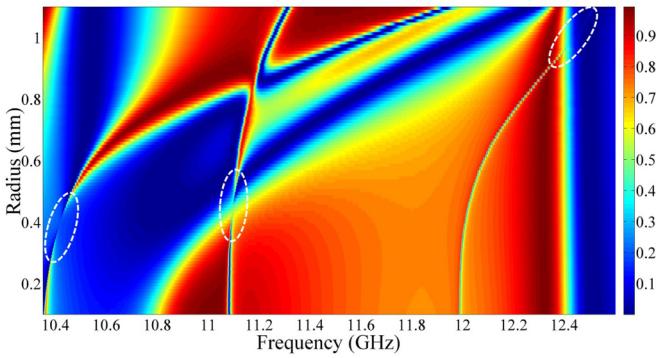

FIG. 4. (Color online) Reflection spectrum $|S_{11}|^2$ between 10.35 and 12.60 GHz (x axis) for an inner radius varying from 0.1 to 1.1 mm (y axis). The outer radius of both resonators is set to 3.5 mm while their respective heights are set to 2.3 mm (resonator 1) and 3.0 mm (resonator 2). Additionally, they are spaced 1.5 mm apart.

We have shown that confinement can be achieved in subwavelength all-dielectric cavities using interference between electromagnetic multipoles and without resorting to metals. The control of multipolar resonances with specific

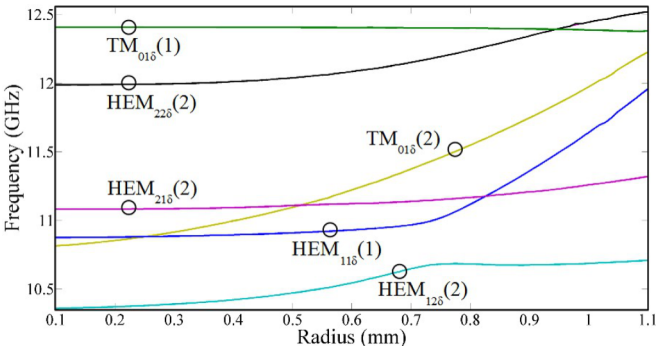

FIG. 5. (Color online) Real part of the S-matrix poles, resonance frequencies, as a function of the radius of resonator 2, for a distance between resonators of 1.5 mm. Five ARCs can be seen to take place. The number in parentheses indicates the resonator to which the mode belongs.

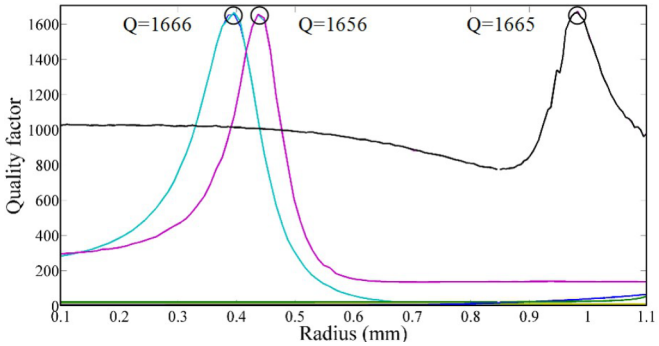

FIG. 6. (Color online) Ratio of real to imaginary parts of S-matrix poles, quality factor, as a function of the radius of resonator 2 for a distance between resonators of 1.5 mm. Radii larger than 500 μm are achievable with current fabrication technology [Fig. 1(c)] [21].

symmetries and their far-field coupling represents an effective method to suppress radiation losses. Multiple bound states in the continuum offer novel design opportunities for applications requiring strong light-matter interaction such as parallel biosensors, compact spectral splitting solar cells, low-threshold nanolasers, single-photon sources, and surface-enhanced Raman scattering sensors. With the recent progress on high-index effective media, this platform can also be transposed to terahertz, infrared, and optics [35]. Mode crossing scenarios offered by the two by two effective Hamiltonians presented here are only a glimpse into the vast and intricate possibilities of multidimensional coupling spaces.

The authors would like to acknowledge the anonymous reviewers for their comments that have considerably improved the quality of the manuscript.

[1] K. Vahala, Nature (London) **424**, 839 (2003).
[2] J. Capmany and D. Novak, Nat. Photonics **1**, 319 (2007).
[3] D. J. Bergman and M. I. Stockman, Phys. Rev. Lett. **90**, 027402 (2003).
[4] A. Jain, P. Tassin, T. Koschny, and C. M. Soukoulis, Phys. Rev. Lett. **112**, 117403 (2014).
[5] J. Zhu, S. K. Ozdemir, Y.-F. Xiao, L. Li, L. He, D.-R. Chen, and L. Yang, Nat. Photonics **4**, 46 (2010).
[6] B. Ellis, M. A. Mayer, G. Shambat, T. Sarmiento, J. Harris, E. E. Haller, and J. Vučković, Nat. Photonics **5**, 297 (2011).
[7] K. L. Tsakmakidis, A. D. Boardman, and O. Hess, Nature (London) **450**, 397 (2007).
[8] J. von Neumann and E. Wigner, Phys. Z. **30**, 465 (1929).
[9] I. Rotter, J. Phys. A: Math. Theor. **42**, 153001 (2009).
[10] H. Friedrich and D. Wintgen, Phys. Rev. A **32**, 3231 (1985).
[11] D. C. Marinica, A. G. Borisov, and S. V. Shabanov, Phys. Rev. Lett. **100**, 183902 (2008).
[12] E. N. Bulgakov and A. F. Sadreev, Phys. Rev. B **78**, 075105 (2008).
[13] F. Monticone and A. Alu, Phys. Rev. Lett. **112**, 213903 (2014).
[14] F. Dreisow, A. Szameit, M. Heinrich, R. Keil, S. Nolte, A. Tünnermann, and S. Longhi, Opt. Lett. **34**, 2405 (2009).
[15] Y. Plotnik, O. Peleg, F. Dreisow, M. Heinrich, S. Nolte, A. Szameit, and M. Segev, Phys. Rev. Lett. **107**, 183901 (2011).
[16] M. I. Molina, A. E. Miroshnichenko, and Y. S. Kivshar, Phys. Rev. Lett. **108**, 070401 (2012).
[17] G. Corrielli, G. Della Valle, A. Crespi, R. Osellame, and S. Longhi, Phys. Rev. Lett. **111**, 220403 (2013).
[18] S. Longhi, Opt. Lett. **39**, 1697 (2014).
[19] C. W. Hsu, B. Zhen, J. Lee, S.-L. Chua, S. G. Johnson, J. D. Joannopoulos, and M. Soljačić, Nature (London) **499**, 188 (2013).
[20] H. Feshbach, Ann. Phys. **19**, 287 (1962); F.-M. Dittes, Phys. Rep. **339**, 215 (2000); N. Auerbach and V. Zelevinsky, Rep. Prog. Phys. **74**, 106301 (2011).
[21] See Supplemental Material at http://link.aps.org/supplemental/10.1103/PhysRevB.90.241103 for details on the effective Hamiltonian formalism, the influence of losses, and experimental results.
[22] A. Figotin and A. Klein, J. Opt. Soc. Am. A **15**, 1423 (1998); P. Kuchment, *Mathematical Modeling in Optical Science* (SIAM, Philadelphia, PA, 2001), Chap. VII; J. D. Joannopoulos, S. G. Johnson, J. N. Winn, and R. D. Meade, *Photonic Crystals, Molding the Flow of Light* (Princeton University Press, Princeton, NJ, 2008), Chap. X; P. M. Morse and H. Feshbach, *Methods of Theoretical Physics, Part I* (McGraw-Hill, New York, 1953), Chap. VI.
[23] S. Fan, P. R. Villeneuve, J. D. Joannopoulos, M. J. Khan, C. Manolatou, and H. A. Haus, Phys. Rev. B **59**, 15882 (1999); Y. Xu, Y. Li, R. K. Lee, and A. Yariv, Phys. Rev. E **62**, 7389 (2000); P. Chak, S. Pereira, and J. E. Sipe, Phys. Rev. B **73**, 035105 (2006); B. Gallinet and O. J. F. Martin, *ibid.* **83**, 235427 (2011).
[24] S. Fan, W. Suh, and J. D. Joannopoulos, J. Opt. Soc. Am. A **20**, 569 (2003); W. Suh, Z. Wang, and S. Fan, IEEE J. Quantum Electron. **40**, 1511 (2004).
[25] B. Luk'yanchuk, N. I. Zheludev, S. A. Maier, N. J. Halas, P. Nordlander, H. Giessen, and C. T. Chong, Nat. Mater. **9**, 707 (2010).
[26] F. R. Ndangali and S. V. Shabanov, arXiv:1108.2003.
[27] N. Hatano, Fortschr. Phys. **61**, 238 (2013).
[28] J. Wiersig, Phys. Rev. Lett. **97**, 253901 (2006).
[29] M. Philipp, P. von Brentano, G. Pascovici, and A. Richter, Phys. Rev. E **62**, 1922 (2000).
[30] E. Persson, I. Rotter, H.-J. Stöckmann, and M. Barth, Phys. Rev. Lett. **85**, 2478 (2000).
[31] S. Zhang, Z. Ye, Y. Wang, Y. Park, G. Bartal, M. Mrejen, X. Yin, and X. Zhang, Phys. Rev. Lett. **109**, 193902 (2012).
[32] A. F Sadreev, E. N. Bulgakov, and I. Rotter, Phys. Rev. B **73**, 235342 (2006).
[33] *Dielectric Resonators*, 2nd ed., edited by D. Kajfez and P. Guillon, (Noble, Atlanta, GA, 1998).
[34] S. P. Shipman and S. Venakides, Phys. Rev. E **71**, 026611 (2005).
[35] X. Yang, J. Yao, J. Rho, X. Yin, and X. Zhang, Nat. Photonics **6**, 450 (2012).